SANDIA REPORT
SAND2001-0811
Unlimited Release
Printed March 2001

An Initial Overview of Iwan Modeling for Mechanical Joints

Daniel J. Segalman

Prepared by
Sandia National Laboratories
Albuquerque, New Mexico 87185 and Livermore, California 94550

Sandia is a multiprogram laboratory operated by Sandia Corporation, a Lockheed Martin Company, for the United States Department of Energy under Contract DE-AC04-94AL85000.

Issued by Sandia National Laboratories, operated for the United States Department of Energy by Sandia Corporation.

Available to DOE and DOE contractors from
U.S. Department of Energy
Office of Scientific and Technical Information
P.O. Box 62
Oak Ridge, TN 37831

Telephone: (865)576-8401
Facsimile: (865)576-5728
E-Mail: reports@adonis.osti.gov
Online ordering: http://www.doe.gov/bridge

Available to the public from
U.S. Department of Commerce
National Technical Information Service
5285 Port Royal Rd
Springfield, VA 22161

Telephone: (800)553-6847
Facsimile: (703)605-6900
E-Mail: orders@ntis.fedworld.gov
Online order: http://www.ntis.gov/ordering.htm

SAND2001-0811
Unlimited Release
March 2001

An Initial Overview of Iwan Modeling for Mechanical Joints

Daniel J. Segalman
Structural Mechanics and Vibration Control Division
Sandia National Laboratories
P.O. Box 5800
Albuquerque, NM 87185-0847

ABSTRACT

The structural dynamics modeling of engineering structures must accommodate the energy dissipation due to microslip in mechanical joints. Given the nature of current hardware and software environments, this will require the development of constitutive models for joints that both adequately reproduce the important physics and lend themselves to efficient computational processes. The exploration of the properties of mechanical joints - either through fine resolution finite element modelling or through experiment - is itself an area of research, but some qualitative behavior appears to be established. The work presented here is the presentation of a formulation of idealized elements due to Iwan, that appears capable of reproducing the important joint properties as they are now understood. Further, methods for selecting parameters for that model by joining the results from experiments in regimes of small and large load are developed. The significance of this work is that a reduced order model is presented that is capable of reproducing the important qualitative properties of mechanical joints using only a small number of parameters.

Acknowledgments

The observations presented in this report grew out of an evolving understanding that could not have taken place without enthusiastic and helpful discussions with fellow Sandians: Jeffrey Dohner, Danny Gregory, David Smallwood, and Todd Simmermacher. Discussion with Danny Gregory and David Smallwood were made especially valuable by their insight into interpretation of experimental results, both their own and those found in the literature. Finally, credit has to be given to the managers, David Martinez, Jamie Moya, and Wendell Kawahara, who have given continuous funding and moral support for this research effort.

Contents

Figures

Mathematical Symbols

a	radius of contact region in Mindlin solution for Hertzian contact indicated in Figure 3. First used in Equation 15.
A_C	total contact area of an interface. First used in Equation 1.
A_S	the portion of the contact area undergoing slip. First used in Equation 1.
A	cross-sectional area in strip-slip calculation indicated in Figure 2. First used in Equation 3.
$B(\ )$	Euler beta function. First used in Equation 14.
c	radius of non-slip region in Mindlin solution for Hertzian contact indicated in Figure 3. First used in Equation 15.
C_p	proportionality coefficient between normal traction and distance along slip length. First used in Equation 11.
C_S	proportionality coefficient between slip length and applied force. First used in Equation 10.
C_u	proportionality coefficient between lateral displacement and distance from tip of slip length. First used in Equation 12.
E	Young's modulus in strip-slip calculation indicated in Figure 2. First used in Equation 3.
D	energy dissipation per cycle. First used in Equation 8.
F_0	amplitude of oscillatory force in harmonic loading. First used in Equation 5.
F_M	maximum applied force magnitude anticipated over a given history. First used in Equation 36.
G	shear modulus. First used in Equation 17.
K_1	stiffness of the soft spring in the augmented Iwan model shown in Figure 5. First used in Equation 52.
K_T	total stiffness of the contact patch. First used in Equation 38.
k	the spring stiffness of the Iwan elements in the networks indicated in Figures 4a and 5. First used in this sense in Equation 28.

$L(t)$ instantaneous length of the slip regime in strip-slip calculation indicated in Figure 2. First used in Equation 5.

N normal traction in strip-slip calculation indicated in Figure 2. First used in Equation 3.

P total normal force. First used in Equation 15.

p_0 average normal traction in contact region in Mindlin solution for Hertzian contact indicated in Figure 3. First used in Equation 16.

$p(x)$ local normal traction at location x. First used in Equation 9.

R multiplicative coefficient in power-law expression for population density of Iwan models. First used in Equation 45.

$U(t)$ total displacement of augmented Iwan network in Figure 5. First used in Equation 52.

$u(x, t)$ displacement in strip-slip calculation indicated in Figure 2. First used in Equation 3.

$u(t)$ displacement of the parallel Iwan elements indicated in Figures 4a and 5. First used in this sense in Equation 27.

x distance from free surface of slip domain. Indicated in Figures 2 and 3.

$x(\phi, t)$ displacement of slider element whose "break free" force is ϕ at time t, indicated in Figures 4a and 5. First used in this sense in Equation 28.

z dimensionless distance from the tip of the slip region in Mindlin solution for Hertzian contact indicated in Figure 3. First used in Equation 17.

z dimensionless distance from the tip of the slip region in Mindlin solution for Hertzian contact indicated in Figure 3. First used in Equation 17.

α exponent in proportionality between normal traction and distance along slip length. First used in Equation 11.

β exponent in proportionality between slip length and applied force. First used in Equation 21.

γ exponent in proportionality between lateral displacement and distance from tip of slip length. First used in this sense in Equation 21.

γ exponent in proportionality between coefficient of friction and normal traction. First used in this sense in Equation 23.

γ exponent in proportionality between dissipation per cycle and applied force. First used in this sense in Equation 26.

ϑ multiplicative coefficient in power-law expression for dissipation resulting from power-law form of population density. First used in this sense in Equation 47.

$\Lambda_n(\theta)$ the nth moment of the population density: $\Lambda_n(\theta) = \int_0^\theta \rho(\phi)\phi^n d\phi$

ν friction coefficient in strip-slip calculation indicated in Figure 2. First used in Equation 3.

$\rho(\phi)$ the population density of Iwan elements whose "break free" force is ϕ. First used in this sense in Equation 28.

$\bar{\phi}$ the value of "break free" force is ϕ selected from the region of overlap between low-force experiments where dissipation data is available and high force experiments where softening data is available.

χ exponent in power-law expression for population density of Iwan models. First used in Equation 45.

Introduction

Constitutive modeling of mechanical joints appears to be gaining increased interest, as indicated by the occurrence of several recent and forthcoming workshops and symposia. That interest would appear to be motivated by the availability of new computational and experimental tools and the perception that the design process for many dynamic systems can be made much more economic by increased reliance on predictive simulation.

This work is driven by the definition that predictive modeling is that which provides reliable quantitative information without first requiring the construction of a prototype. Even this is a matter of degree: Analysis of a design radically different from anything built before requires much more prowess on the part of the analyst to be predictive than does analysis of a design which is a small departure from that which has been built and tested.

Constitutive modeling of mechanical joints is an important part of predictive dynamic modeling of jointed structures because the joints are often the dominant source of energy dissipation and vibration damping in those structures. For very expensive components or components that are safety critical, predictive dynamic modeling is necessary. Jointed structures that fit those criteria include turbine blades and nuclear weapons. The intent of this monograph is to present some ideas that should be directly applicable to the predictive dynamic modeling of such structures for an important regime of excitation - that for which the excitation is sufficient to cause significant energy dissipation but for which the displacements are so minute as to make direct measurement of kinematics impossible. This is the *micro-slip* regime.

Micro-slip at Joints

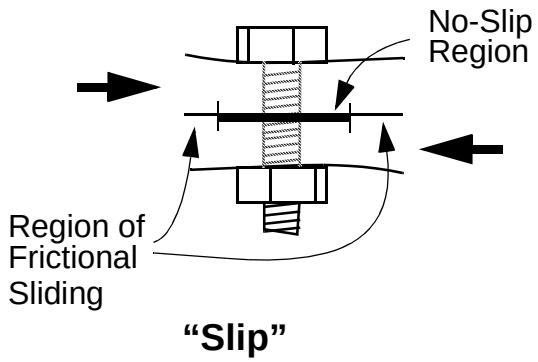

Figure 1. Slip in a joint occurs in a subset of the contact patch.

The notion of micro-slip at a joint is illustrated in Figure 1, where a bolt is used to connect two thick components. There is presumed to be a large prestress in the bolt and a corresponding region of large normal stress between the components in the vicinity of the bolt. A tangential load will cause slip in some region where the normal tractions are not so large as to prevent it. Because slip occurs in a small region, the magnitude of slip displacement is small, and there is no gross slip at the joint; this mechanism is usually described as "micro-slip". The major complication in the analytic prediction of energy dissipation associated with micro-slip is the calculation of the slip region.

The term "micro-slip" is sometimes used interchangeably with the term "partial slip", and this practice has lead to occasional serious misunderstanding. The author would like to suggest that the term "partial slip" should be used for all cases where the slip region is less than the full contact patch - this is any case involving slip short of complete sliding:

$$0 < A_S < A_C \tag{1}$$

where A_S is the area of slip and A_C is the total contact area. The term "micro-slip" should be reserved for cases for which the contact area over which slip occurs is much less than the total contact area:

$$0 < A_S \ll A_C \tag{2}$$

throughout the history of interest.

This importance of this distinction becomes evident when one contrasts convergence studies of micro-slip analysis - which most likely will involve extraordinarily small meshing - with convergence studies of large partial slip.

Dissipation Mechanisms

Energy dissipation at bolted joints has been associated with several distinct mechanisms. This subject was investigated intently by Eric Ungar[1,2] in the early 1960's with an ingenious set of calculations and experiments, studying many factors including joint spacing, joint tightness, flange material and surface finish. Ungar considered oscillatory loads and examined several postulated dissipation mechanisms, computing for each the manner in which energy dissipation would be expected to increase with load. Ungar found that, though there were unknown parameters in those expressions, each mechanism manifested a dissipation rate increasing as a distinct power of the amplitude of the applied load. Ungar then examined experimental data, evaluating the slope of dissipation versus applied force amplitude when plotted in a log-log manner. In those experiments, which concerned thin plates bolted together, Ungar concluded that the dominant mechanism of energy dissipation was air pumping between the plates in the vicinities of the bolted connections. Part of the basis for that conclusion was the observation that the slope of the log-log plot of dissipation versus force was on the order of 2.0, corresponding to viscous dissipation. When the joints were loosened so that there could be significant macro-slip, the slope of the log-log plots increased to 2.5. Ungar's experiments focussed on geometries then most relevant to aircraft bodies. These involved thin plates with

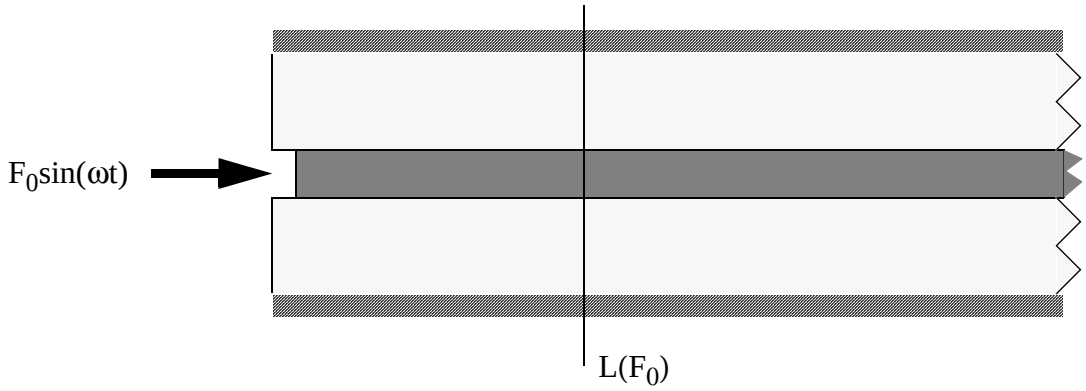

Figure 2. The Goodman hypothesis is illustrated in a one-dimensional problem.

significant bending compliance, and were qualitatively different from the problems of interest here; but Ungar's methods still have value to us. Ungar focused attention on use of the dependence of energy dissipation on amplitude of applied force as a tool to identify dissipation mechanisms.

Where thick sections are bolted together, energy dissipation is generally associated with micro-slip near the bolt and corresponding frictional losses. Goodman[8] observed that several particular calculations of systems that involve slip and Coulomb friction manifested energy dissipation growing as force amplitude to the third power. He generalized that result to that subset of systems of elastic components sharing a frictional interface, held together by a normal force, and perturbed by an oscillatory tangential load for whichthe region of slip increases linearly with the amplitude of tangential force. The derivation will not be developed here, but the core elements are demonstrated by consideration of a semi-infinite rod held in a semi-infinite vise, as shown in Figure 2. The rod is assumed to be elastic and the normal traction applied by the vise is assumed to be uniform. When the applied force is maximum in the cycle, the region of slip is also at its

maximum, extending from the origin to location $L(F_0)$, where F_0 is the amplitude of the oscillatory force. Within the region of slip, the equilibrium equation is:

$$EA\frac{\partial^2 u}{\partial x^2} = 2N\nu \tag{3}$$

where E is Young's modulus, A is cross sectional area of the rod, $u(x)$ is the displacement of the rod at location x, N is the normal traction, and ν is the coefficient of Coulomb friction. (No distinction is made between static and dynamic friction). Note, Poisson contraction is ignored here. Beyond the slip region,

$$u(x) \equiv 0 . \tag{4}$$

Because Equation 3 is second order and L is as yet un-specified, all three of the following boundary conditions are required:

$$u(L) = 0 \; ; \; u'(L) = 0 \; ; \text{and } u'(0) = -F_0/EA \tag{5}$$

The solution at maximum extension is

$$L = \frac{1}{2}\frac{F_0}{N\nu} \tag{6}$$

$$u(x) = \frac{N\nu}{EA}(L-x)^2 \quad \text{for} \quad 0 < x < L \; . \tag{7}$$

The energy dissipation over a full cycle is

$$D = 4\int_0^{L(F_0)} (2N\nu)u(x)dx = \frac{2}{3}\frac{F_0^3}{EA(2N\nu)^2} . \tag{8}$$

This example problem illustrates each of the components that Goodman asserts in his general derivation for problems of oscillatory tangential loads applied to linear objects sharing a frictional interface:

1. the region of slip increases linearly with amplitude of applied load;
2. and the energy dissipation is proportional to the third power of the amplitude of applied force.

Asymptotic Form

Note that in general, in oscillatory loading, the energy dissipation over each cycle is

$$D = 4 \int_0^{L(F_0)} \nu p(x) u(x) dx \tag{9}$$

where $p(x)$ is the normal traction at location x. For the example elasticity problem considered above the slip length, normal traction, and the slip displacement have the forms:

$$L = C_S F_0 \ , \tag{10}$$

$$p(x) = C_p x^{\alpha} \ , \text{and} \tag{11}$$

$$u(x) = C_u (L - x)^{\beta} \ . \tag{12}$$

The energy dissipation is

$$D = 4\nu C_p C_u \int_0^{L(F_0)} x^{\alpha} (L - x)^{\beta} dx \tag{13}$$

$$= [4\nu C_p C_u C_S^{\alpha + \beta + 1} B(\alpha + 1, \beta + 1)] F_0^{\alpha + \beta + 1} \tag{14}$$

where $B(\ )$ is the Euler beta function[3].

For the example considered above, $\alpha = 0$, $\beta = 2$, and $\alpha + \beta + 1 = 3$ (satisfying the Goodman hypothesis).

Goodman used the problem of contacting spheres subject to small lateral slip to illustrate his observation about frictional dissipation. That problem, having normal force P and

lateral force F_0, contact radius a, and no-slip radius c, is illustrated in the following figure.

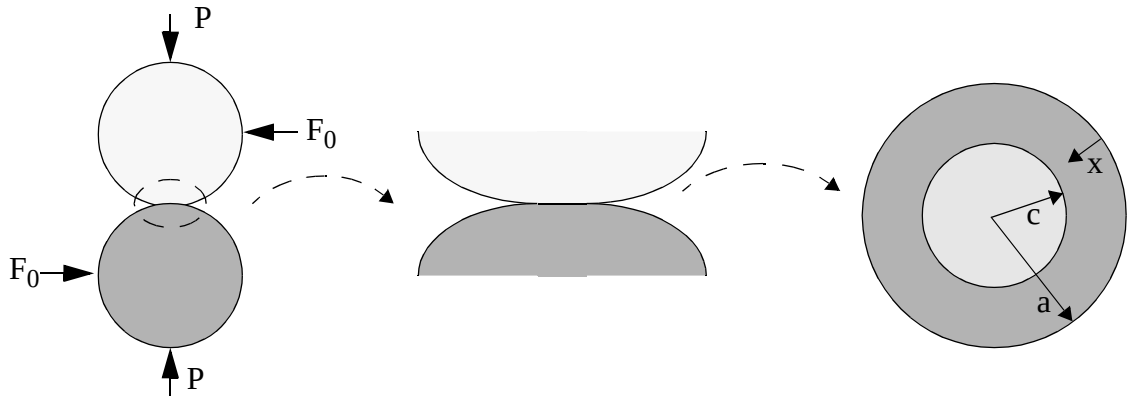

Figure 3. The geometry of Hertzian contact.

The coordinate from the free surface toward the slip/no-slip interface is indicated by x. For that problem, whose solution was worked out by Mindlin[4] and Cattaneo[5] independently, the closed form solutions are provided by Johnson[6]:

$$\frac{c}{a} = \left(1 - \frac{F_0}{\nu P}\right)^{1/2}, \tag{15}$$

$$p(x) = p_0\left(1 - \left[1 + \frac{x}{a}\right]^2\right)^{1/2}, \tag{16}$$

$$\text{and } u(x) = \frac{3\nu P}{16Ga}(2-\mu)\left\{\left(1 - \frac{2}{\pi}\text{asin}\frac{1}{1+z}\right)\left(1 - 2\left(\frac{1}{1+z}\right)^2\right) + \frac{2}{\pi}\frac{1}{1+z}\left(1 - \left(\frac{1}{1+z}\right)^2\right)^{\frac{1}{2}}\right\}, \tag{17}$$

where $p_0 = 2\frac{P}{\pi a}$, μ is Poisson's ratio, G is shear modulus, and $z = \frac{(a-c)-x}{c}$. Note that cz is the distance from the slip/no-slip interface to location x. For the case of micro-slip (expressed in this case by $(a-c)/c \ll 1$), the above expressions can be written:

$$a - c = \frac{aF_0}{2\nu P}, \tag{18}$$

$$p(x) = p_0 (x/a)^{1/2}, \tag{19}$$

and

$$u(x) = \frac{\nu P}{Ga}(2-\mu)\frac{\sqrt{2}}{\pi} z^{3/2}. \tag{20}$$

So here we see that the slip length is again proportional to the lateral load. We also identify $\alpha = 1/2$, $\beta = 3/2$, and observe that $\alpha + \beta + 1 = 3$ again.

Experimental results are generally disappointing for the analyst. In general, the experimentalists do find that micro-slip yields a power-law relationship between lateral load and energy dissipation, but they tend to find exponents closer to 2.5 rather than 3.0. (Johnson(1961) and Ungar(1967)). Various explanations have been offered, most of which come down to the assertion that Coulomb friction may not be an adequate model for the dissipation taking place in the slip region. Johnson (*ibid*) asserts that the true dissipation involves metal plasticity not accounted for by Amonton's law. Gaul (1997) suggests that the calculation of dissipation in the region of small normal stresses requires direct accounting for asperity to asperity interaction, resulting in a different kind of friction law. Recent experiments at Sandia National Laboratories by Smallwood, Gregory and Coleman (2000) suggest values between 2.6 and 2.9 for the power-law relationship between lateral load and energy dissipation. The construction of low-order models both for the case of slope 3.0 and for cases for slope less than 3.0 is discussed below.

There are various ways that the conditions of Goodman's analysis can be weakened and still yield a power-law relation between tangential load and dissipation. In particular, α

and β need not sum to 2. Further, the relationship between tangential load and the length of the slip region need not be linear. If the slip region is related to the maximum amplitude of the tangential load in the following manner,

$$L \propto F_0^{\gamma} \tag{21}$$

then analysis such as that which leads to Equation 14 yields

$$D \propto F_0^{\gamma(\alpha+\beta+1)}. \tag{22}$$

A more interesting case is that in which the pressure and displacement results of the classical solutions are preserved, but that the friction law is altered. This exploration is consistent with the observation that micro-slip occurs in regions of very low normal traction where Amonton's law might not be valid. It is anticipated that some other physics apply in the regime of low normal tractions and that as the normal traction is increased that behavior gradually converges into Coulomb friction. One model of friction in the region of low pressure involves pressure dependent friction coefficients (Rabinowicz, 1995), the simplest of which is

$$\nu(p) = \nu_0\left(\frac{p}{p_0}\right)^{\gamma}. \tag{23}$$

The dissipation becomes

$$D = 4\nu_0 C_u (C_p^{1+\gamma}/p_0^{\gamma}) L^{\alpha+\beta+1} L^{\alpha\gamma}. \tag{24}$$

If we accept the portion of the Goodman assertion that $\alpha + \beta = 2$ and that $L = C_L F$, then we find that

$$D \propto F_0^{3+\alpha\gamma}. \tag{25}$$

If the friction law used above is a good approximation for reality when γ is a slightly negative number, this result becomes valuable on two counts:

- the model supports the deviation of experiment from Goodman's hypothesis in the correct direction;
- the model predicts a different power-law relationship for each type of contact (spherical contact, plate contact, strip contact). We now have some predictions to test against experiment.

Whether Equations 11, 12, 23 can adequately describe the physics of joint slip is still a matter of research. Ideally, a continuum level (finite element) model, properly accommodating all of the relevant physics could explain power-law dissipation relations and determine the relevant parameters.

The above discussion has explored methods by which either analytic elasticity or finite element tools can be employed to derive an expression for dissipation of the form

$$D = AF_0^{\gamma} \tag{26}$$

and methods for predicting appropriate values of the parameters A and γ. We shall see below that these quantities are enough to determine parameters for limited constitutive models for jointed structures.

Model Reduction

Whatever physics hold in joint interfaces, detailed solution of those equations as part of a finite element model for the whole structure would introduce hundreds of new unknowns for each joint, each unknown associated with a nonlinear equation. Further,

capturing those degrees of freedom would be associated with extremely small elements, dramatically reducing the characteristic time step of the problem. These limitations make such an approach impractical. Instead, one strives to devise low order models - on the order of tens of degrees of freedom - to represent the region of the structure surrounding the joint. The small number of associated nonlinear equations should not substantially add to the numerical difficulty of the problem.

The utility of a reduced order model depends substantially on the difficulty of deriving parameters of the model. In general, it would be quite acceptable to devise a very fine scale model of the joint and to use that fine scale model to perform a small number of experiments sufficient to deduce the parameters of a lower order model. Alternatively, it might be just acceptable to compile experimental data from which model parameters could be deduced for each geometric and loading condition.

Discrete Models

Though one might be satisfied using a mesh of elements of characteristic length on the order of tens of microns in order to understand or characterize a joint, it would be impractical to incorporate this mesh into the larger one used to simulate that overall structure of which the joint is a small part. Instead one attempts to represent the complex joint problem with a reduced model of lumped parameters. The most common class of model is that composed of springs and slider elements. Slider elements manifest the properties of Coulomb friction:

$$\dot{u} = \begin{cases} 0 & \text{if} \quad |f| < \phi \\ \lambda \, \mathrm{sgn}(f) & \text{if} \quad |f| > \phi \end{cases} \tag{27}$$

where f is the force applied on the slider element, u is the resulting displacement, ϕ is a "break-free force", and λ is a positive number selected to meet kinematic boundary conditions. Such networks appear to have been studied first in connection with constitutive modeling of metal plasticity, and it was in that connection that Iwan wrote his most often cited paper [9] on parallel-series and series-parallel networks of springs and sliders. Iwan derived analytic expressions for the stress-strain behavior of each sort of

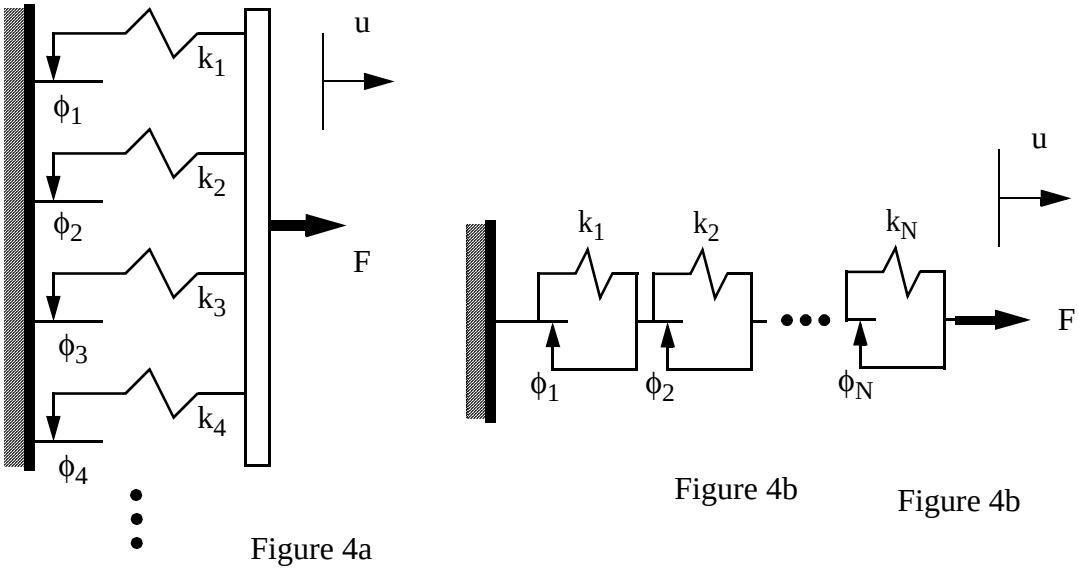

Figure 4a Figure 4b Figure 4b

Figure 4. Iwan parallel-series systems (a) and series-parallel systems (b).

network. Of particular interest is the special case of parallel-series networks where there are an infinite number of spring-slider units and the stiffnesses of all the units are identical, k. Let $\rho(\phi)$ be the population density of sliders of break-free force ϕ. After an arbitrary displacement, the force on the system will be

$$F(t) = \int_0^\infty \rho(\phi) k[u(t) - x(\phi, t)] d\phi \tag{28}$$

where $x(\phi, t)$ is the current displacement of sliders of species ϕ.

Since solution of this problem requires calculating the evolution of $x(\phi, t)$ over time for each ϕ, we must specify initial conditions as well as evolution equations. Before lateral loads are imposed on the structure,

$$x(\phi, t) = 0 \text{ at } t = 0 \text{ for all } \phi . \tag{29}$$

The slider displacements, $x(\phi, t)$, are considered hidden variables; they might be deduced, but they cannot be measured directly.

The force associated with an initial unidirectional displacement of the network is

$$F(u) = \int_0^{ku} \phi \rho(\phi) d\phi + ku \int_{ku}^{\infty} \rho(\phi) d\phi . \tag{30}$$

Iwan showed that the distribution density can be calculated from the force-displacement curve of this initial deformation

$$k^2 \rho(\phi) = \left. \frac{\partial^2 F}{\partial u^2} \right|_{ku = \phi} . \tag{31}$$

Sanliturk and Ewins [10] used the above reasoning to derive a corresponding finite difference expression.

Where the initial force-displacement curve is unavailable, other methods must be exploited. Gaul and Lenz[11] performed a series of dynamic experiments exploiting resonance of a two mass system connected by a mechanical joint. Having only steady state data, they selected from combinations of various mechanical elements - springs, dampers, slider elements - to reproduce the mechanical properties of the joint as manifest in those dynamic experiments with good success.

We now consider a parallel-series network such as Iwan investigated, each element

having the same stiffness, but in series with a single, relatively soft spring (stiffness K_1). In this model, the parallel Iwan model is meant to represent the contact region and the soft spring is meant to represent the rest of the joint. Because the Iwan network is in series with

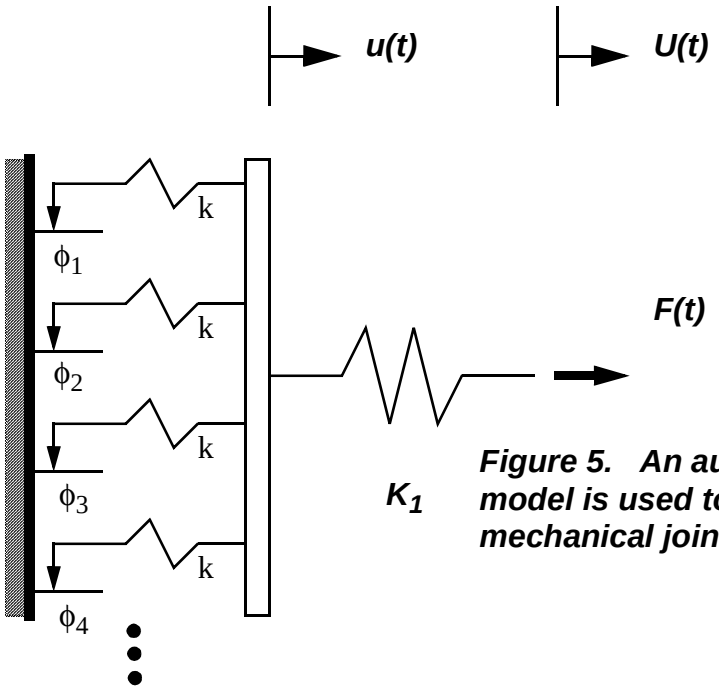

Figure 5. An augmented Iwan model is used to represent a mechanical joint.

the soft spring, Equation 28 still applies. Now, however, the displacement, $u(t)$, associated with the Iwan system is a hidden variable. Only the net system displacement, $U(t)$, and net applied load, $F(t)$, can be measured.

For the above and in what follows, it is convenient to define the moments of the distribution as

$$\Lambda_n(\theta) = \int_0^\theta \rho(\phi)\phi^n d\phi . \tag{32}$$

The dimension of $\Lambda_n(\theta)$ is that of θ^n.

It is also worthwhile to note that the force necessary to cause full slip of the joint is

expressed both in terms of the first moment of ρ and the normal load

$$\Lambda_1(\infty) = \nu P \tag{33}$$

thus at least this feature of ρ can be determined experimentally.

Iwan's Equation 30 for monotonic loading still holds for the augmented model of Figure 5. In terms of the moments, that expression becomes

$$F(t) = \Lambda_1(ku(t)) + ku(t)[\Lambda_0(\infty) - \Lambda_0(ku(t))] \ . \tag{34}$$

If one knew the density function, ρ, the above integral equation could be solved for $u(t)$ in terms of $F(t)$.

Iwan's Equation 31 also holds, but could be useful only where experiment yielded forces such that the second derivative on the right hand side of that equation resulted in meaningful values. This is particularly unlikely where applied loads are small. Another difficulty with exploitation of this equation is that, in general, one does not know the values of u that correspond to each value of F. More will be said on this issue later in this monograph.

Energy Dissipation Due to Harmonic Loading

Here we are not restricted to actual sinusoidal loading, just that which increases monotonically from a value of $-F_A$ to F_A and then decreases monotonically back to $-F_A$. The energy dissipation associated with a cycle is four times that associated with the motion from the origin to the extreme position and due to the work done by the sliding elements

$$D = 4\int_0^{ku_A} \phi(u_A - \phi/k)\rho(\phi)d\phi$$
$$= 4\left[u_A\Lambda_1(ku_A) - \frac{1}{k}\Lambda_2(ku_A)\right]. \quad (35)$$

At this stage, the hidden state u_A appearing above is the maximum displacement due to the applied periodic load and is still an unknown.

Limit of Small Force

We consider the limit of displacements due to very small loads - this is the region of micro slip - characterized by the existence of a bound F_M such that

$$F(t) < F_M \quad (36)$$

for all times and that

$$\int_0^{F_M/K_T} \rho(\phi)d\phi \ll \int_{F_M/K_T}^{\infty} \rho(\phi)d\phi \quad (37)$$

where

$$K_T = k\Lambda_0(\infty). \quad (38)$$

This is different from, but consistent with the condition that the applied load is much less than the load necessary to cause macro-slip

$$F \ll \nu P = \Lambda_1(\infty). \quad (39)$$

We now expand Equation 34 in terms of small ku and find

$$F(t) = ku(t)\Lambda_0(\infty) + O(u^{2+\chi})$$
$$= K_T u(t) + O(u^{2+\chi}). \quad (40)$$

We can substitute this into our expression for energy dissipation due to harmonic loading

$$D(F_0) \cong 4\left[\frac{F_0}{K_T}\Lambda_1\left(\frac{kF_0}{K_T}\right) - \frac{1}{k}\Lambda_2\left(\frac{kF_0}{K_T}\right)\right]$$
$$= \frac{4}{k}\int_0^z (z-\phi)\phi\rho(\phi)d\phi \quad . \tag{41}$$

where $z = kF_0/K_T$. We see that in the domain of micro-slip, it is only the behavior of $\rho(\phi)$ in the vicinity of $\phi = 0$ which affects the dissipation per cycle. The constitutive model constructed for the configuration shown in Figure 5 can be applied to arbitrary load histories, and it would be desirable to deduce the parameters of this constitutive model from simple experiments, such as that of harmonic loading.

Case of Smooth Distribution:

We consider the case of any distribution that is smooth near $\phi = 0$. For such distributions, we employ a Taylor series

$$\rho(\phi) = \rho_0 + \rho_1\phi + \ldots \tag{42}$$

then

$$\Lambda_1(\beta) \cong \rho_0\beta^2/2$$
$$\Lambda_2(\beta) \cong \rho_0\beta^3/3 \tag{43}$$

and

$$D \cong \frac{2\rho_0 k^2}{3}\left(\frac{F_0}{K_T}\right)^3. \tag{44}$$

The above supports the Goodman hypothesis that the dissipation in cyclic loadings will be proportional to the cube of the peak loading force.

Case of Singular Distribution

Next, we remove the constraint that the distribution $\rho(\phi)$ be smooth for small ϕ. We consider distributions that have the form

$$\rho(\phi) \cong R\phi^{\chi} \tag{45}$$

for small values of its argument. The moments become

$$\Lambda_n(\phi) = R\phi^{\chi+n+1}/(\chi+n+1), \tag{46}$$

and Equation 41 for energy dissipation due to harmonically applied loads becomes

$$D = \frac{4R}{k}\frac{(F_0/\Lambda_0(\infty))^{\chi+3}}{(\chi+2)(\chi+3)} = \frac{4R}{k}\frac{(F_0 k/K_T)^{\chi+3}}{(\chi+2)(\chi+3)} = \vartheta F_0^{\chi+3} \quad . \tag{47}$$

The above demonstrates that a weak singularity of $\rho(\phi)$ near $\phi = 0$, $(-1 < \chi < 0)$, will yield a power law dissipation of the order sometimes claimed for the micro-slip domain. Note that when χ has the value 0, Equation 47 reduces to Equation 44 and ρ_0 has the value R.

We are now left with the challenge of deducing the parameters of the distribution in terms of measurable quantities, so much as possible. The exponent χ can be deduced from the slope of a log-log plot of dissipation due to harmonic loading versus the amplitude of that loading

$$\chi = \frac{d}{d\log F_0}\log D - 3. \tag{48}$$

We show below how, within the regime of micro-slip, the rest of the parameters for our constitutive model can be determined from the harmonic loading experiment.

The big question is how to choose the parameters. Once the physics is decided, the

exponent χ is fixed. The hard question is how to determine R (ρ_0 in the case $\chi = 0$), k, and K_T. One strategy would be to devise some other class of experiment with the intention that these new experiments would further identify the individual parameters that go into making up υ. We consider an experiment in which a large force is applied to the joint and then released:

- the elastic compliance of the overall joint drowns out the deflections due to interface slip during extension
- after release, the residual displacement is due solely to interface mechanics

This suggests that experiments relating the residual deformation and the amplitude of the applied load or the displacement during the loading portion of the experiment might help resolve the problem of identifying the remaining parameters. As shown in Appendix A, for the case where $\chi = 0$, the resulting residual deformation is related to the maximum deformation by

$$u_R = \frac{1}{4}\left(\frac{\rho_0 k^2}{K_T^3}\right) F_M^2 \tag{49}$$

where u_R is the residual deformation and F_M is the maximum loading. We see that the parameters ρ_0, k, and K_T group together in the same manner in this problem as they do in the calculation of dissipation under oscillatory loading.

This suggests that the individual values of R (ρ_0 in the case $\chi = 0$), k, and K_T do not matter in the dissipation modeling of the joint; that what matters is the manner in which these parameters come together to form the quantity $\vartheta = \frac{4R}{k}\frac{(k/K_T)^{\chi+3}}{(\chi+2)(\chi+3)}$. (Note that the individual values of the parameters will make a difference in the values of the hidden

variables; those values will not be observable from macroscopic scale experiments.)

The above assertion is argued mathematically in Appendix B and supported by a numerical experiment using parameters as indicated in the following table:

Table 1: Parameters of two Iwan Models

	F_{max}	Iwan Elements	Time Steps	ρ_0	k	KT	$\vartheta = \frac{2\rho_0 k^2}{3K_T^3}$	Resulting Dissipation
Case 1	1.0	50	2000	4.0	0.5	1000	6.66667E-10	2.74149E-10
Case 2	1.0	50	2000	2.0	2.0	2000	6.66667E-10	2.74159E-10

The number of elements and the number of time-steps is gross over-kill for the problem at hand, but were selected in order to assure that the difference in the predictions of the two cases was due only to the intrinsic mathematical difference due to selecting different combinations of R, k, and K_T that combine to the same value of ϑ. The imposed load in this test case is a sum of sine functions of different period and amplitude

$$F(t) = \frac{1}{2}\left(\sin\left((t) + \frac{1}{2}\sin(6t)\right)\right) \tag{50}$$

and is shown in Figure 6. This load was selected to be significantly different from a simple harmonic loading. In particular, there are significant load reversals on each side of the zero-crossings.

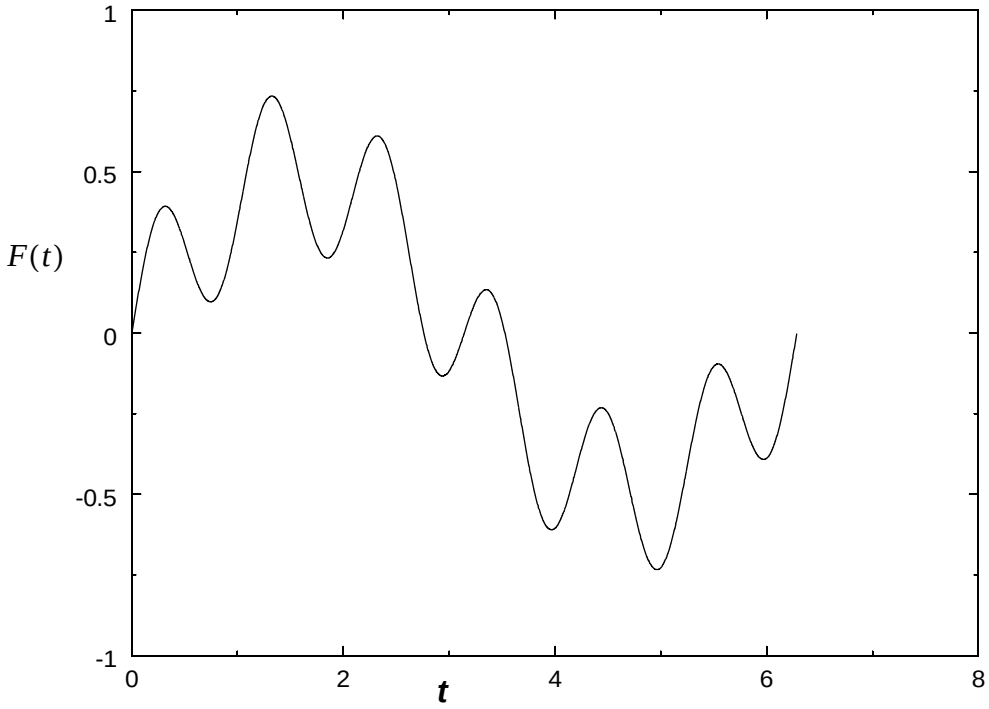

Figure 6. Test case using non-sinusoidal applied force

$$F(t) = \frac{1}{2}\left(\sin(t) + \frac{1}{2}\sin(6t)\right)$$

The resulting time derivatives of the hidden variable u are shown in Figure 7. Because the product $\rho_0 k$ of Case 1 is half that of Case 2, the displacements of Case 1 are double those of Case 2.

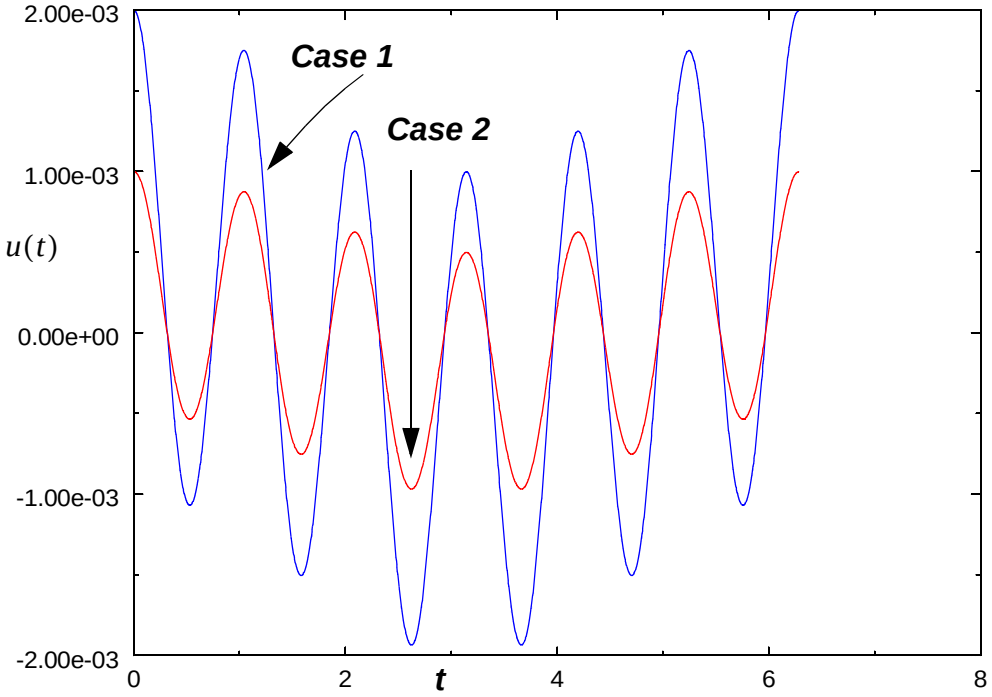

Figure 7. Resulting time derivative of displacement u(t)

The net force due to the slipping Iwan elements is shown in Figure 8. We see that the forces of Case 1 are just about half of those of Case 2.

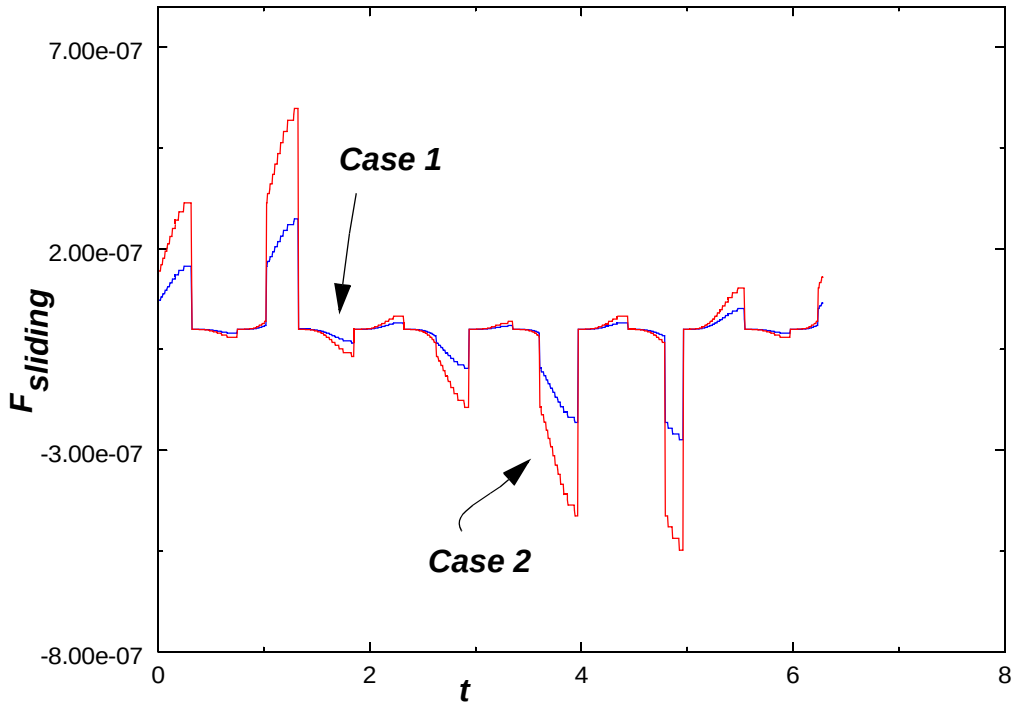

Figure 8. Instantaneous net force from all sliding Iwan elements.

The instantaneous energy dissipation is that due to motion of the sliding elements. This is the product of the forces in Figure 8 times the displacement rates of Figure 7. Those dissipation rates are shown in Figure 9. The dissipation rates for Cases 1 and 2 are identical and superpose.

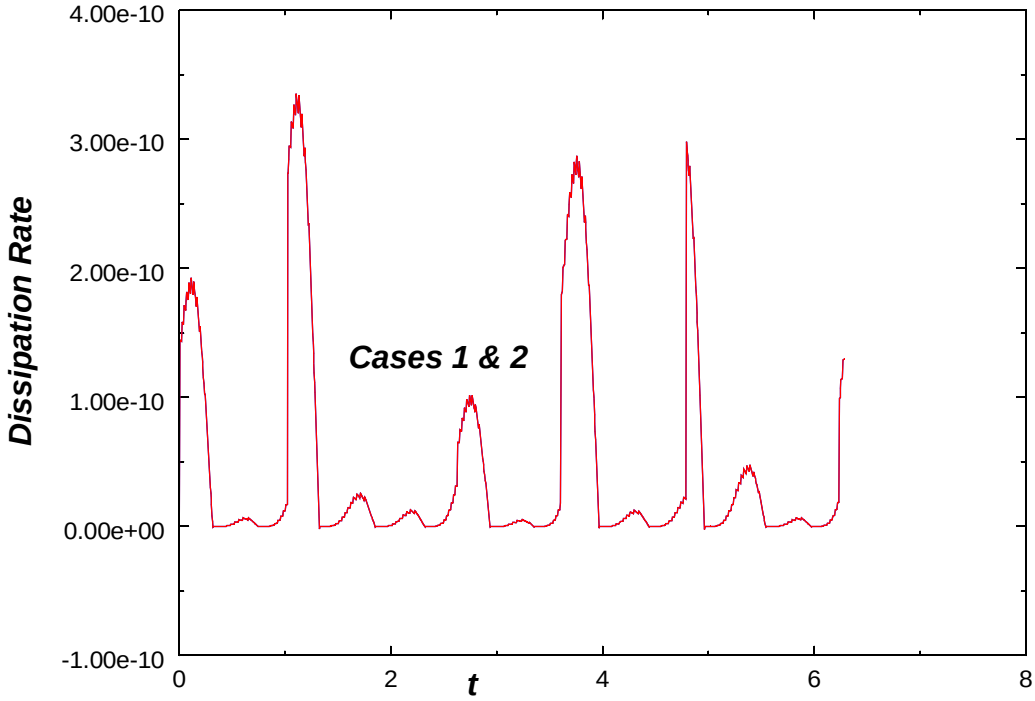

Figure 9. Resulting dissipation rates are identical for both cases.

We conclude from the above discussion that in the domain of small applied loads, the distribution $\rho(\phi)$ behaves as a fractional negative power of its argument. Further, though the model parameters χ, υ, and K_1 are defined uniquely, we are free to select the model parameters, R, k, and K_T arbitrarily so long as

$$\frac{4R}{k}\frac{(k/K_T)^{\chi+3}}{(\chi+2)(\chi+3)} = \upsilon \tag{51}$$

and the dissipative nature of the system will be preserved. Note that varying the values of R, k, and K_T does change the magnitudes of the hidden displacements u and $\{x_k\}$.

Note that the above discussion applies to the region of small applied forces, where clean data on the force-displacement relationships is hard to obtain but where dissipation versus amplitude data is available. It is in the correspondingly small values of ϕ that $\rho(\phi)$

behaves as a power of its argument.

Large Force Response

It is shown above how experiments involving small oscillatory loads can provide information on $\rho(\phi)$ for small values of its argument through consideration of dissipation. Here, we see how estimates for $\rho(\phi)$ for large values of its argument can be obtained through considerations of a different sort.

One expects the force-displacement curve for large monotonic loading to look something like that in the following figure. In the regime of small loads (micro-slip), the

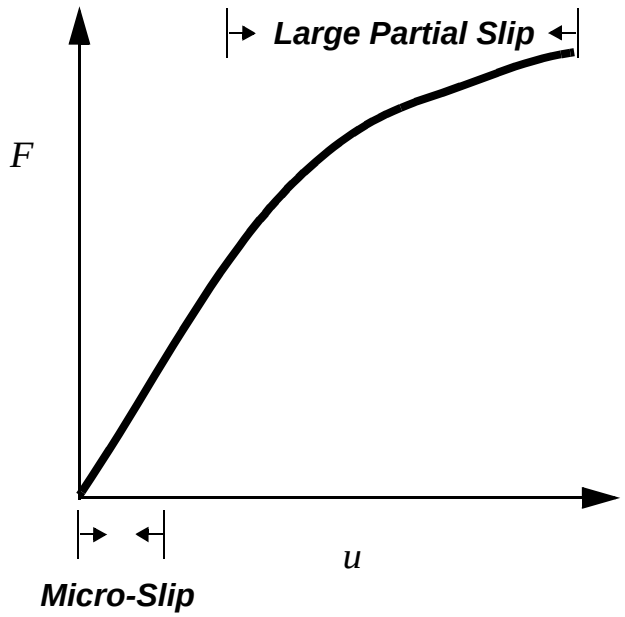

Figure 10. Force-displacement curve for large monotonic loading

curve is nearly linear and little information can be deduced from the curvature. More importantly, in the region of small loads, there is no practical method to deduce $u(t)$ from the observable joint quantities, U and F. Though, in principle, one could solve the following equation

$$u(t) = U(t) - F/K_1 \tag{52}$$

for u, evaluation of that equation would involve looking for nearly in-perceptible differences between experimental values.

The problem simplifies a bit in the region of large displacements - well beyond the region of micro-slip. In that region, one could use the above equation to get realistic values of $u(t)$ from U and F. We may now plot F versus u and evaluate the curvature of the plot numerically to estimate $\rho(\phi)$ for large values of its argument via Equation 31. Note that in these experiments u is no longer a hidden variable.

Note also that the model parameter k appears in Equation 31 and is still to be assigned a unique value.

Model Parameters

Selecting Parameters

The model parameters χ and υ are defined uniquely in terms of dissipation experiments at low amplitude. The parameter K_1 is uniquely determined from small amplitude force-displacement experiments. The remaining parameters, R, k, and K_T, can be chosen arbitrarily to match the dissipation at small force amplitude so long as Equation 51 is satisfied. This arbitrariness is disturbing. Also, it would be desirable to define $\rho(\phi)$ over the full range of its argument. These issues can be resolved in the following manner.

1. Set $k = 1$. This is equivalent to making the change of variables $\rho(\phi) = \tilde{\rho}(\phi/k)/k^2$ in Equations 28 and 31.
2. Equation 31 can now be used unambiguously to determine a plot of $\rho(\phi)$ versus ϕ for large values of ϕ.
3. Let $\bar{\phi}$ be the minimum value of ϕ for which the above process yields reliable values of ρ.

4. Select R so that $R\bar{\phi}^{\chi}$ matches the value $\rho(\bar{\phi})$ obtained from Equation 31.

5. Use Equation 51 to determine K_T.

6. Use $\rho(\phi) = R\phi^{\chi}$ for $\phi < \bar{\phi}$ and use $\rho(\phi)$ obtained from Equation 31 for $\bar{\phi} < \phi$.

Discretization of the Model

The continuous Iwan model is characterized by the two numbers K_T and k and the function $\rho(\phi)$. Here we discuss how one may approximate the continuous Iwan model, whose parameters can be determined by the methods above, by a finite system of discrete Iwan elements.

Discretization of the continuous Iwan system is most economically done by using only as many Iwan elements as necessary. Lets assume that the experiments we contemplate simulating involve loads for which F_M is an upper bound. One can employ Equation 30 to plot F versus u for monotonically applied loads and thereby to find a corresponding u_M. The constitutive equation may now be evaluated numerically by breaking the domain of integration $(0, \infty)$ into the two domains $(0, ku_M)$ and (ku_M, ∞). The Iwan model becomes

$$F = \int_0^{ku_M} k(u - x(\phi))\rho(\phi)d\phi + ku\int_{ku_M}^{\infty} \rho(\phi)d\phi$$

$$= \int_0^{ku_M} k(u - x(\phi))\rho(\phi)d\phi + u\left[K_T - k\int_0^{ku_M} \rho(\phi)d\phi\right]. \quad (53)$$

We now approximate the above integral by a summation over discrete points

$$\rho(\phi) \cong \sum \rho(\phi)\delta(\phi - \phi_j)\Delta\phi_j . \tag{54}$$

When Equation 54 is substituted into Equation 53, one obtains

$$F(t) \;=\; k\sum \rho(\phi_j)[u(t) - x_j(t)]\Delta\phi_j + u(t)\hat{K}_T \tag{55}$$

where dependence on time is shown explicitly and $\hat{K}_T$ is the quantity in the brackets in Equation 53.

Numerical experiments for the case $\chi \;=\; 0$, presented below, have been reasonably successful with a uniform distribution of sample points. Slightly negative values of χ might be well suited by a distribution consistent with some other quadrature strategy.

An example of the above strategy is presented in Appendix B.

Conclusions

1. A number of plausible reasons can be put forth for why the Goodman analysis of micro-slip in joints fails quantitatively and yet is vindicated in predicting a power-law relationship between applied lateral force and energy dissipation.
2. Iwan elements do appear to be natural candidates for joint models since they possess the physical qualities of elasticity and slip associated with joint mechanics.
3. Distributions of Iwan elements can be devised that will reproduce the power-law behavior at small amplitude that is found experimentally.
4. Experimental data from dissipation measurements at small loads and force-displacement measurements at large load can be used to determine all the necessary model parameters.
5. Numerical simulation with the distributions of Iwan elements can be performed quickly and efficiently.

References

1. Ungar, Eric E., “Energy dissipation at structural joints; mechanisms and magnitudes”, Technical Documentary Report No. FDL-TDR-64-98, Air Force Flight Dynamics Laboratory, Wright-Patterson Air Force Base, Ohio, 1964.

2. Ungar, E.E., “The status of engineering knowledge concerning the damping of built-up structures”, *Journal of Sound and Vibration, 26,* 1973, pp. 141-154.

3. Lebedev, N. N., *Special Functions and Their Applications*, rev. English ed. New York: Dover, 1972.

4. Mindlin, R.D., “Compliance of elastic bodies in contact”, *J. Appl. Mech*., 16, 1949, 259-268.

5. Cattaneo, C., “Sul contatto di due corpi elasticiti: distribuzione locale degli sforzi”, *Rendiconti dell’ Accademia naxionale dei Lincei, 27,* Ser. 6, 1938, p. 214

6. Johnson, K.L., *Contact mechanics*, Cambridge University Press, 1985

7. Johnson, K.L., ‘Energy dissiopation at spherical surfaces in contact transmitting oscillating forces”, Journal of Mechanical Engineering Sciences, 3, 1961, p 362

8. Goodman, L. E., “A review of progress in analysis of interfacial slip damping”, *Structural Damping*, papers presented at a colloquium on structural damping held at the ASME annual meeting in Atlantic City, NJ, December, 1959, edited by Jerome E. Ruzicka, pp. 35-48.

9. Iwan, W. D., “On a class of models for the yielding behavior of continuous composite systems”, *Journal of Applied Mechanics, 89*, 1967, pp. 612-617.

10. Sanliturk, K. Y. and D. J. Ewins, “Modelling two-dimensional friction contact and its application using harmonic balance method”, *Journal of Sound and Vibration, 193,* 1996, pp. 511-523.

11. Gaul, L. and J. Lenz, “Nonlinear dynamics of structures assembled by bolted joints”, *Acta Mechanica, 125*, 1997, pp. 169-181.

12. Rabinowitcz, E., Friction and Wear of Materials, John Wiley and Sons, New York,

1995, pp 69-71.

13. Pierre, C., A. A. Ferri, and E. H. Dowell, “Multi-harmonic analysis of dry friction damped systems using an incremental harmonic balance method”, Journal of Applied Mechanics, 52, 1985, pp. 958-964.

14. Sanliturk, K. Y., M. Imregun, and D. J. Ewins, “Harmonic balance vibration analysis of turbine blades with friction dampers”, *Journal of Vibration and Acoustics, 119,* 1997, pp. 96-102.

15. Smallwood, D. O., D. L. Gregory, and R. G. Coleman, “Damping Investigations of a Simplified Frictional Shear Joint”, *Preceedings of the 71st Shock and Vibration Symposium,* Alexandria VA, Nov. 2000.

16. Menq, C.-H., J. Bielak, and J. H. Griffin, “The influence of microslip on vibratory response, part 1: a new microslip model”, *Journal of Sound and Vibration, 107,* 1986, pp. 279-293.

This Page Intentionally Left Blank

Appendix A: The Residual Slip Experiment

We next consider the slip captured after a monotonically applied force which achieves its maximum at a value F_M. Equation 30 provides the relationship between that applied force and the resulting displacement u_1. (Recall that u_1 is a hidden variable; $u_1 \ll 1$) The distribution of slider displacement is

$$\begin{aligned} x(\phi, t_1) &= u_1 - (\phi / k) \qquad \text{for} \qquad \phi < k u_1 \\ x(\phi, t_1) &= 0 \qquad\qquad\qquad\quad \text{for} \qquad k u_1 < \phi \end{aligned} \tag{A1}$$

where t_1 is the moment at which the applied load reaches its maximum. Of course, the imposed displacement associated with the elasticity of the overall joint disappears when the applied load is removed and a residual displacement u_R associated with interface slip remains. The problem is illustrated in the following figure.

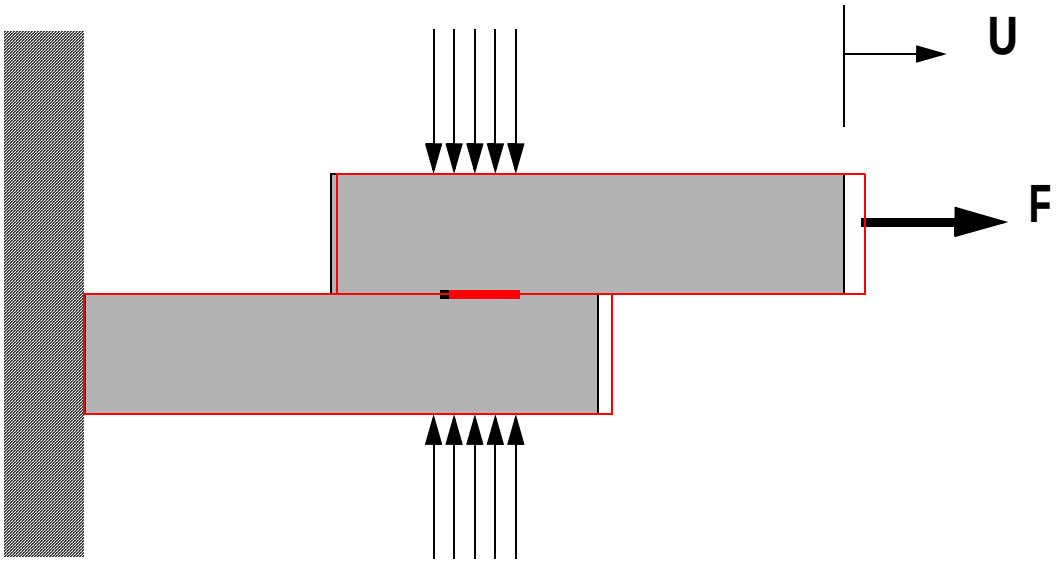

Figure A1. The problem of residual deformation.

Let's solve for u_R in terms of the applied load.

At time t_2, after the load is removed, there is no load in the soft spring and the residual displacement is u_R. At that time, the distribution of slider displacement is

$$\begin{aligned} x(\phi, t_2) &= u_R + \phi/k && \text{for} \quad \phi < k\left(\frac{u_1 - u_R}{2}\right) \\ x(\phi, t_2) &= u_1 - (\phi/k) && \text{for} \quad k\left(\frac{u_1 - u_R}{2}\right) < \phi < ku_1 \\ x(\phi, t_2) &= 0 && \text{for} \quad ku_1 < \phi \end{aligned} \quad . \qquad \text{(A2)}$$

The slip values for time t_1 and t_2 are shown in Figure A2.

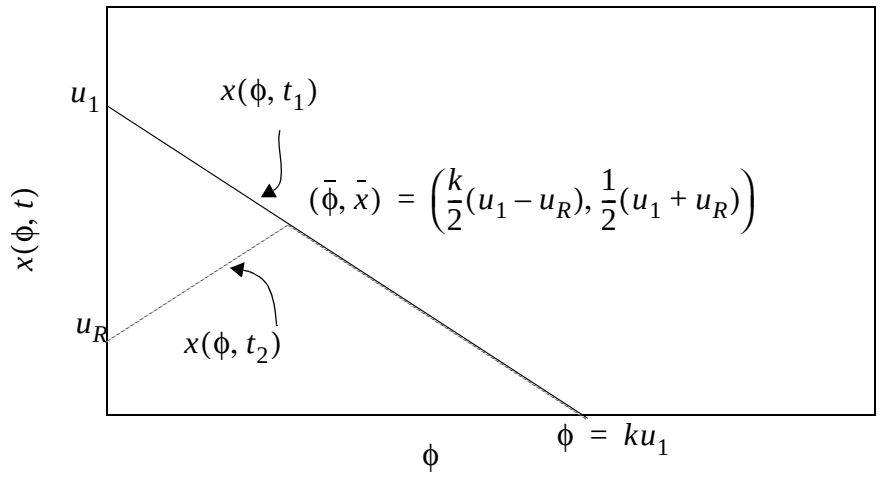

Figure A2. Slip distribution during the forward motion of the joint and after force on the joint has been released.

Substituting zero-force into Equation 28, we find an expression to solve for u_1 in terms of u_R

$$u_R K_T = \int_0^{\bar{\phi}} (ku_R + \phi)\rho(\phi)d\phi + \int_{\bar{\phi}}^{\bar{ku_1}} (ku_1 - \phi)\rho(\phi)d\phi \qquad \text{(A3)}$$

where $\bar{\phi} = \frac{k}{2}(u_1 - u_R)$.

When we approximate $\rho(\phi) = \rho_0$ for small ϕ, we may solve for u_1 in terms of u_R

$$u_1 = -u_R + \frac{2}{\rho_0 k}[4\rho_0 K_T u_R - 2(\rho_0 k u_R)^2] \tag{A4}$$

For very small u_1 and u_R,

$$u_1 = 2\left(\frac{K_T u_R}{\rho_0 k^2}\right)^{1/2}. \tag{A5}$$

Finally, we exploit the assumption of small slip (Equation 40) to observe that

$$u_1 = F_M / K_T \tag{A6}$$

so that residual displacement u_R can be expressed in terms of the applied load

$$u_R = \frac{1}{4}\left(\frac{\rho_0 k^2}{K_T^3}\right) F_M^2. \tag{A7}$$

Note that the quantity in parenthesis is the same combination of parameters that occurs in the expression for dissipation resulting from harmonic tangential loading.

This Page Intentionally Left Blank

Appendix B: Significance of the Dissipation Parameter

In Equation 47, ϑ relates the rate of dissipation due to harmonic loading to a power of the amplitude of the applied load. Here we establish, that where the "small force" assumption is employed so that the distribution function $\rho(\phi)$ can be represented adequately by its behavior near zero (Equation 45) and by the integral defining K_T (Equation 38), it does not matter how the parameters k, K_T, and R are chosen so long as the correct ratio for $\vartheta = \frac{4R}{k}\frac{(k/K_T)^{\chi+3}}{(\chi+2)(\chi+3)}$ is achieved. In the next appendix, it is shown how to determine the appropriate values of ϑ from finite element calculation.

We consider two distinct Iwan systems. The first is characterized by the parameters k, K_T, and R and the second by the parameters $\tilde{k}$, $\tilde{K}_T$, and $\tilde{R}$. Re-using the scalars α, β, and γ, we assume the relationships

$$\begin{aligned} \tilde{K}_T &= \alpha K_T \\ \tilde{k} &= \beta k \\ \tilde{R} &= \gamma R \end{aligned} \quad . \tag{B1}$$

The symbols α, β, and γ are reused here because of the small size of the Greek alphabet and have nothing to do with their earlier use in the body of this monograph.

Each system is subject to the identical load history $F(t)$ where $F(t)$ is always less than some F_M and the hidden displacements are expressed to first order as

$$u(t) = F(t)/K_T \qquad \tilde{u}(t) = F(t)/\tilde{K}_T \tag{B2}$$

The integrands ϕ and $\tilde{\phi}$ range over $(0, ku_M)$ and $(0, k\tilde{u}_M)$, respectively. Setting

$$\frac{\phi}{ku_M} = \frac{\tilde{\phi}}{k\tilde{u}_M} \tag{B3}$$

from which follows

$$\tilde{\phi} = \frac{ku_M}{k\tilde{u}_M}\phi = \frac{\beta}{\alpha}\phi . \tag{B4}$$

We now relate the slider displacements $x(\phi, t)$ and $\tilde{x}(\tilde{\phi}, t)$ of the two systems. Say that instantaneously the following holds

$$\tilde{x}(\tilde{\phi}, t) = \frac{1}{\alpha}x(\phi, t) . \tag{B5}$$

We shall show that the time derivatives of each of these quantities are such as to maintain compliance with Equation B5. The sliders are either moving or not and we consider each case individually. Say the slider at ϕ is not moving $(\dot{x}(\phi, t) = 0)$ then

$$k|u - x(\phi, t)| < \phi \Rightarrow \quad \frac{\beta}{\alpha}k|u - x(\phi, t)| < \frac{\beta}{\alpha}\phi \Rightarrow \quad \tilde{k}\left|u - \tilde{x}(\tilde{\phi}, t)\right| < \tilde{\phi} \tag{B6}$$

and we see that $\dot{\tilde{x}}(\tilde{\phi}, t) = 0$ also. On the other hand, say that the slider at ϕ is moving, then

$$k|u - x(\phi, t)| = \phi \Rightarrow \quad \frac{\beta}{\alpha}k|u - x(\phi, t)| = \frac{\beta}{\alpha}\phi \Rightarrow \quad \tilde{k}\left|u - \tilde{x}(\tilde{\phi}, t)\right| = \tilde{\phi} \tag{B7}$$

and

$$\dot{x}(\phi, t) = \dot{u}(t) \Rightarrow \frac{1}{\alpha}\dot{x}(\phi, t) = \frac{1}{\alpha}\dot{u}(t) \Rightarrow \dot{\tilde{x}}(\tilde{\phi}, t) = \frac{1}{\alpha}\dot{x}(\phi, t) . \tag{B8}$$

Since the displacement of all sliders begin's with the same initial value (zero), we see that

$$\tilde{x}(\tilde{\phi}, t) \equiv \frac{1}{\alpha}x(\phi, t) . \tag{B9}$$

We now examine the instantaneous rate of dissipation

$$d(t) = \int_0^{ku_M} \dot{x}(\phi, t)\phi\rho(\phi)d\phi = R\dot{u}(t)\int_0^{ku_M} \psi(\dot{\chi}(\phi, t))\phi^{1+\chi}d\phi \tag{B10}$$

where $\psi(\dot{\chi}(\phi, t))$ is a characteristic function of its argument, defined as

$$\psi(\xi) = 0 \quad \text{when} \quad \xi = 0$$
$$\psi(\xi) = 1 \quad \text{when} \quad \xi \neq 0 \,. \tag{B11}$$

Similarly,

$$\tilde{d}(t) = \int_0^{k\tilde{u}_M} \dot{\tilde{x}}(\tilde{\phi}, t)\tilde{\phi}\tilde{\rho}(\tilde{\phi})d\tilde{\phi} = \tilde{R}\dot{\tilde{u}}(t) \int_0^{k\tilde{u}_M} \psi(\dot{\tilde{\chi}}(\tilde{\phi}, t))\tilde{\phi}^{1+\chi} d\tilde{\phi}$$
$$= \frac{\gamma}{\beta}\left(\frac{\beta}{\alpha}\right)^{3+\chi} R\dot{u}(t) \int_0^{ku_M} \psi(\dot{\chi}(\phi, t))\phi^{1+\chi} d\phi = \frac{\gamma}{\beta}\left(\frac{\beta}{\alpha}\right)^{3+\chi} d(t) \,. \tag{B12}$$

The above asserts that the two systems will indistinguishable in their dissipation properties so long as

$$\frac{\gamma}{\beta}\left(\frac{\beta}{\alpha}\right)^{3+\chi} = 1 \,. \tag{B13}$$

Satisfaction of Equation B13 is equivalent to the assertion that the systems will be indistinguishable so long as they are associated with the same value of ϑ

$$\tilde{\vartheta} = \frac{4\tilde{R}}{\tilde{k}} \frac{(\tilde{k}/\tilde{K}_T)^{\chi+3}}{(\chi+2)(\chi+3)} = \left(\frac{\gamma}{\beta}\right)\left(\frac{\beta}{\alpha}\right)^{3+\chi}\left(\frac{4R}{k} \frac{(k/K_T)^{\chi+3}}{(\chi+2)(\chi+3)}\right) = \vartheta \,. \tag{B14}$$

This Page Intentionally Left Blank

Appendix C: Example Finite Element Calculation

If one has a prototype of an isolated joint, one can perform harmonic experiments at different amplitudes to obtain a linear plot of force versus displacement (from which K_1 can be obtained) and a log-log plot of dissipation versus force amplitude (from which χ and ϑ can be obtained). From ϑ and χ, one constructs an Iwan model in the manner described in the body of this monograph.

Alternatively, one can devise a detailed finite element mesh for the joint and solve the fine-scale contact problem assuming a reasonable friction law, usually Coulomb friction. The following example calculations were performed using the Sandia finite element code JAS on a mesh created with the help of the Sandia code CUBIT. The joint mesh is indicated in Figures C1 through C3. Approximately three hundred thousand degrees of freedom were employed in this model.

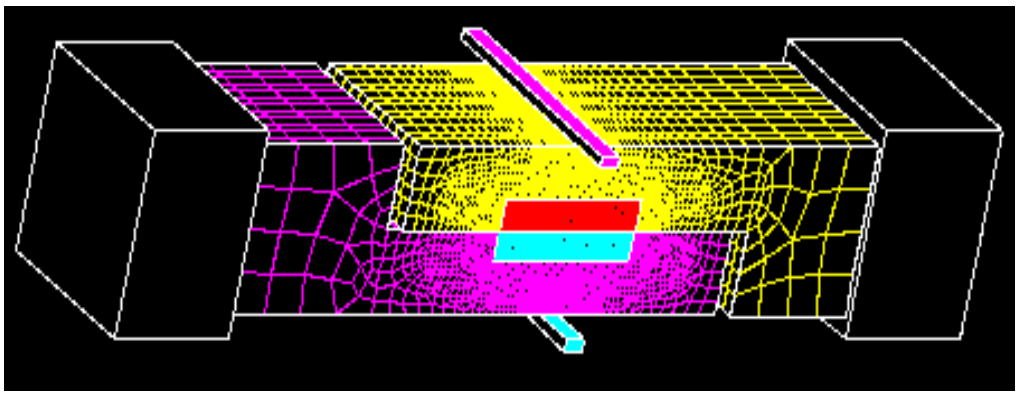

Figure C1. A mesh of a simple lap joint. The rounded rods on the top and bottom are portions of rigid rollers pushing the laps together.

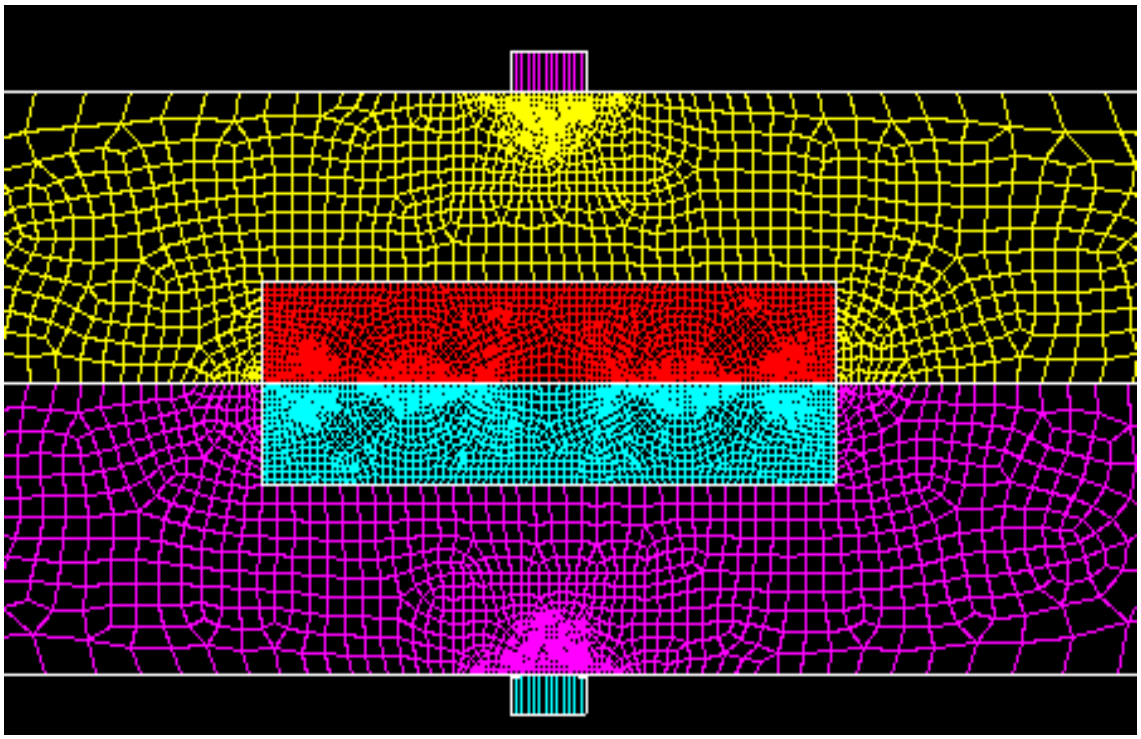

Figure C2. A magnified view of the mesh of the previous figure.

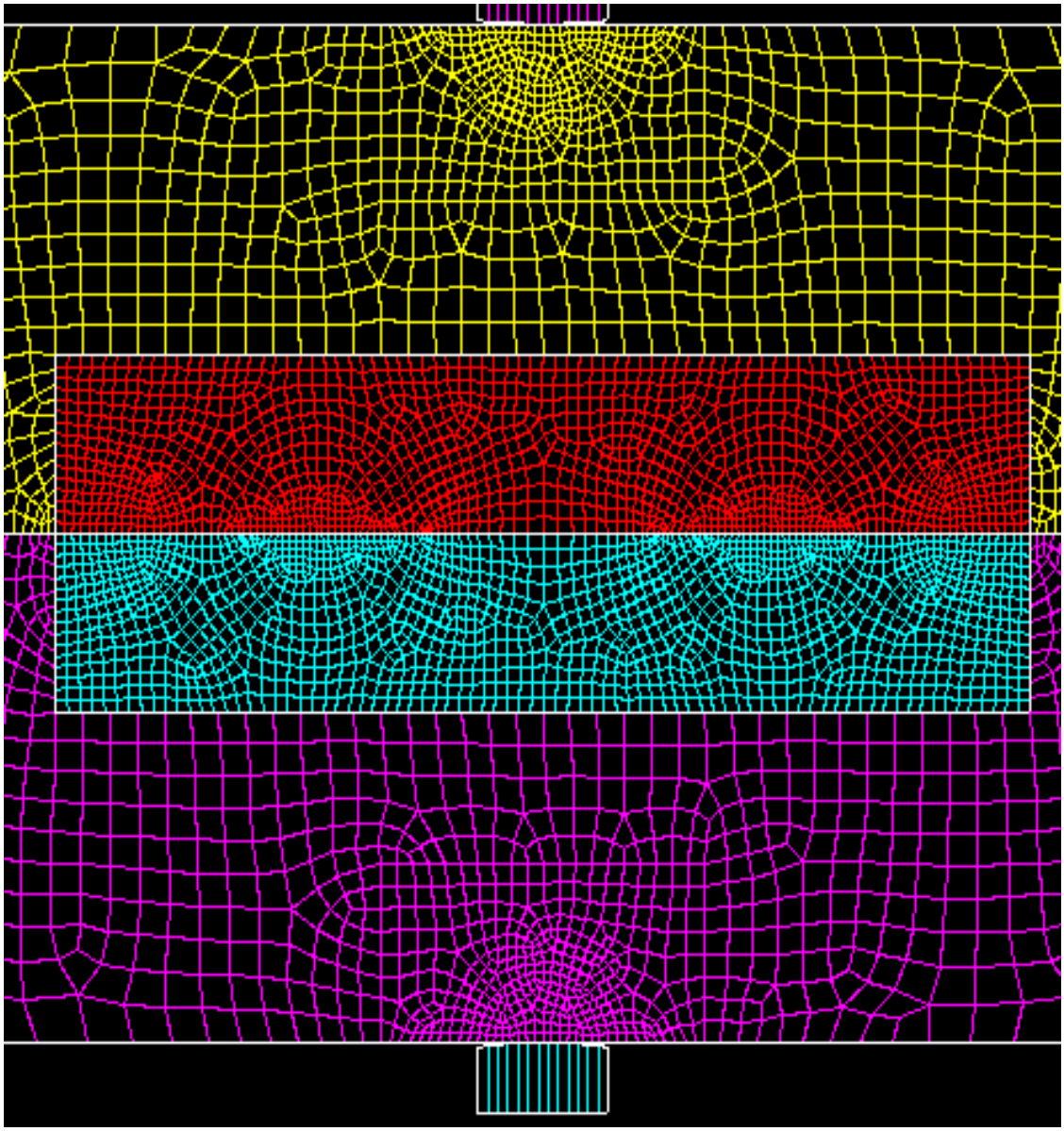

Figure C3. A further magnified view of the finite element mesh.

Vertical loads of 1.78 x10^8 dynes (400 pounds force) are applied by rollers to push the laps together and the laps are then pulled apart under displacement control. The force

resulting displacements curve is plotted in the following figure.

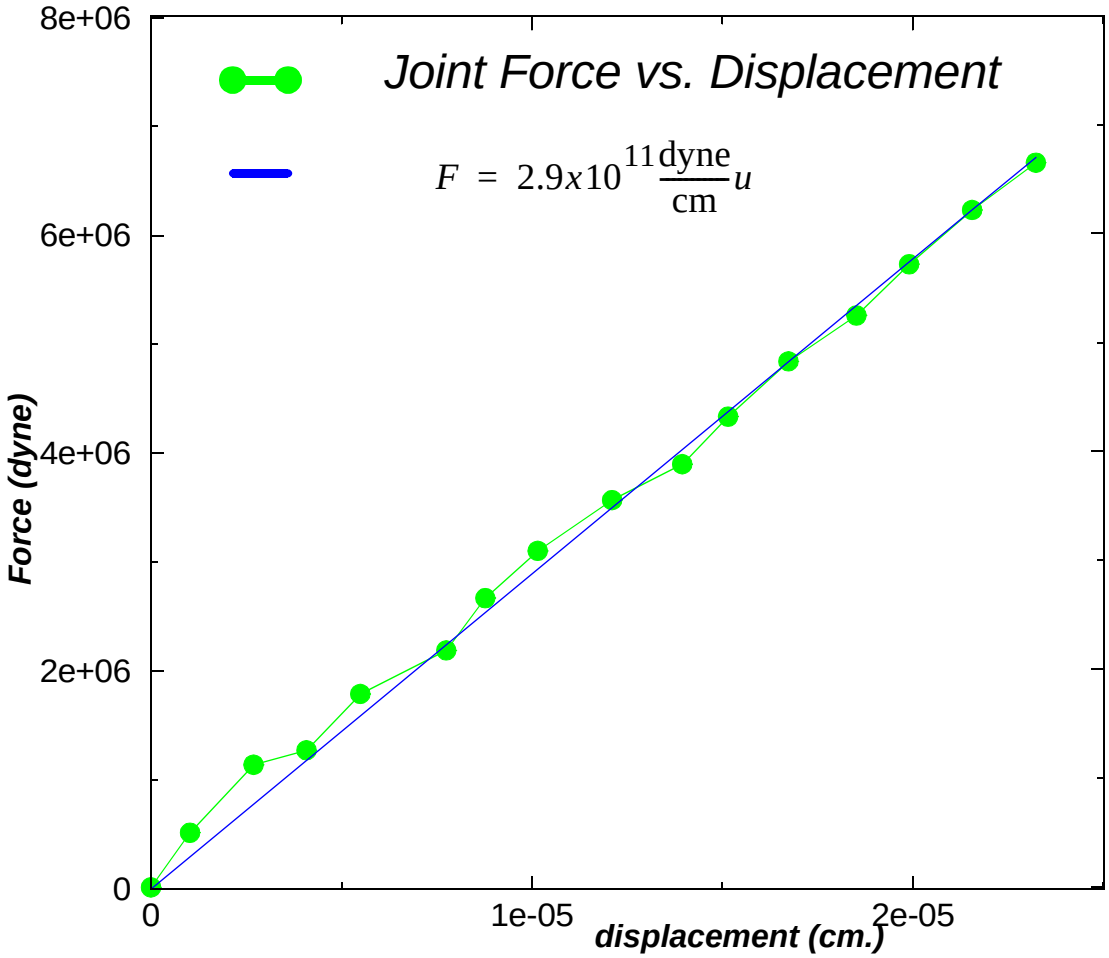

Figure C4. The force displacement curve can be matched reasonably well with a straight line. The slope of this line is K_1**.**

The plot of dissipation versus applied force is shown in the following figure,

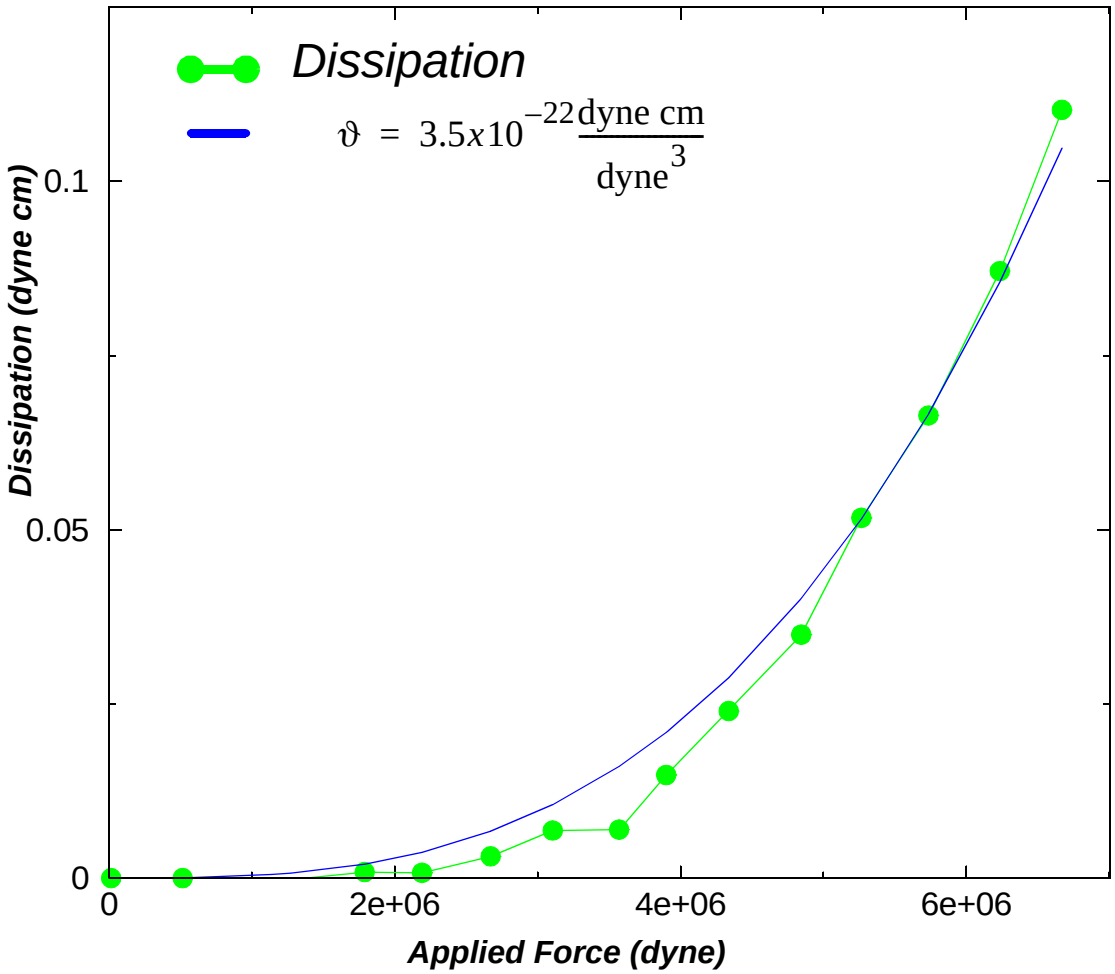

Figure C5. Dissipation associated with monotonically applied force is used to deduce the dissipation ratio ϑ.

Having the two parameters K_1 and ϑ, we now have the necessary parameters to create an appropriate Iwan model

Distribution

1	MS 9018	Central Technical Files,	9845-1
2	MS 0899	Technical Library,	9616
1	MS 0612	Review & Approval Desk, For DOE/OSTI	9612
1	MS 0841	Bickel, Thomas C	9100
1	MS 0824	Ratzel, Arthur C	9110
1	MS 0847	Morgan, Harold S	9120
1	MS 0824	Moya, Jaime	9130
1	MS 0827	McGlaun, J Michael	9140
1	MS 9042	Kawahara, Wendell	8725
1	MS 9042	Dawson, Dan	8725
1	MS 9042	Antoun, Bonnie	8725
1	MS 0557	Baca, Thomas J	9125
1	MS 0557	Gregory, Danny Lynn	9125
1	MS 0847	Martinez, David R.	9124
5	MS 0847	Dohner, Jeffery	9124
1	MS 0847	Smallwood, David	9124
10	MS 0847	Segalman, Daniel J.	9124

1 Prof. Lawrence Bergman
Univ. of Illinois
Aero/Astro Engr.
Urbana, IL 61801

1 Prof. Alexander F. Vakakis
Department of Mechanical
& Industrial Engineering
104 Mechanical Engineering Building,
MC-244
1206 West Green Street
Urbana, IL 61801

1 Prof. Xiaomin Deng
Department of Mechanical Engineering
University of South Carolina
Columbia, SC 29208

1 Prof. Lee Peterson
University of Colorado at Boulder
Campus Box 429
Boulder, CO 80309-0429

1 Prof. K.C. Park
University of Colorado at Boulder
Campus Box 429
Boulder, CO 80309-0429

1 Dr. Marie Levine
Jet Propulsion Laboratory (JPL)
Science and Technology
Development Section
4800 Oak Grove Drive
Pasadena, CA 91109-8099

1 Prof. Edward J. Berger
Dept. Mech. & Industrial Engr.
University of Cincinnati
PO Box 210072
Cincinnati, OH 45221-0072